

Quark-nova remnants III: Application to RRATs

Rachid Ouyed¹, Denis Leahy¹, Brian Niebergal¹, and Youling Yue^{1,2}

¹Department of Physics and Astronomy, University of Calgary, 2500 University Drive NW, Calgary, Alberta, T2N 1N4 Canada

²Astronomy Department, School of Physics, Peking University, Beijing 100871, China

received/accepted

Abstract. This is the third paper of a series of papers where we explore the evolution of iron-rich ejecta from quark-novae. In the first paper, we explored the case where a quark-nova ejecta forms a degenerate shell, supported by the star's magnetic field, with applications to SGRs. In the second paper we considered the case where the ejecta would have sufficient angular momentum to form a degenerate Keplerian torus and applied such a system to two AXPs, namely 1E2259+586 and 4U0142+615. Here we explore the late evolution of the degenerate torus and find that it can remain unchanged for $\sim 10^6$ years before it becomes non-degenerate. This transition from a degenerate torus (accretion dominated) to a non-degenerate disk (no accretion), occurs about 10^6 years following the quark-nova, and exhibits features that are reminiscent of observed properties of RRATs. Using this model, we can account for the duration of both the radio bursts and the quiet phase, as well as the observed radio flux from RRATs. The unique on and off activity of the radio pulsar PSR B1931+24 is similar to that of “old RRATs” in our model. For old RRATs, in our model, the spin-down rate during the radio loud phase is about a factor 1.6 larger than when it is quiet, remarkably similar to what has been measured for PSR B1931+24. We discuss a connection between XDINs and RRATs and argue that some XDINs may be “dead RRATs” that have already consumed their non-degenerate disk.

Key words. accretion, accretion disks – (stars:) pulsars: general – dense matter – X-rays: bursts – Elementary particles

1. Introduction

McLaughlin et al. (2006) have recently reported the detection of eleven “Rotation Radio Transients”, or “RRATs”, characterised by repeated, irregular radio bursts, with burst durations of 2-30 ms, and intervals between bursts of ~ 4 min to ~ 3 hr. The RRATs are concentrated at low Galactic latitudes, with distances implied by their dispersion measures of $\sim 2 - 7$ kpc. For ten of the eleven RRATs discovered by McLaughlin et al. (2006), an analysis of the spacings between repeat bursts reveals an underlying spin period, P , and also in three cases, a spin period derivative, \dot{P} . The observed periods fall in the range $0.4 \text{ s} < P < 7 \text{ s}$, which generally overlap with those seen for the radio pulsar population. Since August 2003, all the sources have been reobserved at least nine times at intervals of between one and six months (i.e. they show sporadic radio bursting for years). All have shown multiple bursts, with between 4 and 229 events detected in total from each object (see Table 1 in McLaughlin et al. (2006)). For the three RRATs with values measured for both P and \dot{P} , a characteristic age, τ_c , and a dipole surface magnetic field, B , can be inferred and are listed in Table 1. The total number of these objects is a few times that previously estimated for all radio pulsars (McLaughlin et al. (2006)).

The discovery of the first X-ray counterpart to a RRAT was reported by Reynolds et al. (2006) for RRAT J1819–1458. The X-ray spectrum detected by Chandra and XMM-Newton is thermal, fit well by a blackbody with $kT \sim 0.1$ keV with a possible excess at high energies. Combined with the high inferred surface magnetic field strength, long spin period, and lack of persistent radio emission this led to a comparison with the population of magnetars (e.g. Reynolds et al. (2006)). These comparative studies showed the obvious differences between magnetars and RRATs: (i) the magnetar birth rate is well below that estimated for the RRAT population (Popov et al. (2006)); (ii) X-ray properties of RRATs seem distinct from those seen for magnetars: RRATs seem much colder and less luminous than the magnetars, and apparently lacks the hard X-ray tail seen for these sources (e.g. Gaensler et al. (2007), Rea (2007)); (iii) X-ray temperature of RRATs is around 0.1-0.2 keV below the average 0.5 keV associated with magnetars.

The lack of persistent radio emission and the long spin period of at least one RRAT has raised the possibility of a link between XDINs (Haberl 2004)¹ and RRATs. Furthermore, Popov et al. (2006) show that the inferred birthrate of RRATs is consistent with that of XDINs but not with magnetars. The XDINs are slightly cooler ($kT \sim 0.04 - 0.1$ keV) and less lumi-

¹ No radio emission of any kind has been reported from XDINs; recent observations (Bradley 2006) show no RRAT-like radio bursts toward RX J0720.4–3125 (or toward magnetars).

nous ($L_X \sim 10^{31} - 10^{32}$ ergs s $^{-1}$) than J1819–1458. However, the measured period derivatives of two XDINs (RBS 1223 and RX J0720.4–3125; Kaplan & van Kerkwijk 2005a, 2005b), and the detection of possible proton cyclotron lines in their spectra (van Kerkwijk 2004), imply magnetic field strengths similar to those of J1819–1458. The immediate questions are (i) why only one RRAT shows X-rays as the XDINs do, and (ii) why XDINs do not show any radio emission (latest searches for pulsed and bursty radio emission from XDINs led to no detection despite of their proximity compared to RRATs; Kondratiev et al. (2007)).

RRAT J1819–1458 properties in the X-ray show similarities to those of radio pulsars with ages around 100 kyr. For example, PSR J0538+2817 is 30 kyr old and has $kT_\infty = 160$ eV, while PSR B0656+14 is 110 kyr old and has $kT_\infty = 70$ eV (see Reynolds et al. (2006) for details). However, the inferred surface magnetic field strength of RRATs is at least an order of magnitude greater than the radio sources. Two radio pulsars with comparable magnetic fields that have been detected in X-rays are PSRs J1718–3718 (Kaspi and McLaughlin (2005)) and J1119–6127 (Gonzalez et al. (2005)). These sources show temperatures ($kT \sim 150 - 200$ eV) and luminosities ($\sim 10^{32} - 10^{33}$ ergs s $^{-1}$) comparable to that of RRAT J1819–1458, although both sources are probably much younger (35 and 1.7 kyr, respectively) and, in contrast to RRAT J1819–1456, have X-ray luminosities less than their spin-down luminosities.

1.1. Literature explanations

The models proposed so far in the literature can be classified into the following categories: (i) Extreme pulses from distant pulsars (Weltevrede et al. (2006)), similar to the pulses seen from the nearby pulsar B0656+14. (ii) Re-activated radio pulsars (Zhang et al. (2007)) where the RRATs are pulsars that are no longer active, but for which a temporary “star spot” with multipole field components emerges above the surface. This magnetic field component could temporarily reactivate the radio beaming mechanism, producing the observed bursts. (iii) Nulling pulsars viewed from the opposite direction (Zhang et al. (2007)). In this model, RRATs are normal pulsars with their magnetic poles not aligned favorably for detection, but undergo an magnetic reversal and so occasionally produce emission that can be observed. (iv) Sporadic accretion (Cordes and Shannon (2006), Li (2006)). Here the RRAT mechanism might be produced by interaction of the neutron star with an equatorial fallback disk or with orbiting circum-polar debris. Accretion from a disk should quench the radio emission mechanism, but sporadic drops in the accretion rate could allow the radio beam to turn on for a fraction of a second, producing the RRAT phenomenon (Li (2006)).

In this paper, the third of a series, we present an alternative scenario that incorporates SGRs, AXPs, XDINs, and RRATs into one family of compact objects. In our model, SGRs, AXPs, XDINs, and RRATs are all strange quark stars that differ, for the most part, only by age.

This paper is organized as follows: Sect. 2 describes our strange quark star model. Sect. 3 discusses the implications of

the evolution of debris material left over from the birth of the strange quark star. In Sect. 4 we show how after roughly one million years the debris can become responsible for RRAT behaviour. Then, in Sect. 5 we describe observations and make predictions using our model. We discuss some further implications of our model in Sect. 5, and lastly we conclude in Sect. 6.

2. Our model

In the quark-nova (QN) picture (Ouyed et al. (2002), Keränen et al. (2005); hereafter ODD and KOJ respectively) the core of a neutron star, that undergoes the phase transition to the quark phase, shrinks in a spherically symmetric fashion to a stable, more compact strange matter configuration faster than the overlaying material (the neutron-rich hadronic envelope) can respond, leading to an effective core collapse. The core of the neutron star is a few kilometers in radius initially, but shrinks to 1-2 km in a collapse time of about 0.1 ms (Lugones et al. (1994)). The gravitational potential energy released (plus latent heat of phase transition) during this event is converted partly into internal energy and partly into an outward propagating shock wave that imparts kinetic energy to the overlying material.

As described in a series of papers (Ouyed et al. (2007a), Ouyed et al. (2007b); hereafter referred to as OLN I and OLN II), during a quark-nova the degenerate crust of a neutron star is blown off, leaving behind a strange quark star (QS) surrounded by left over, highly-metallic degenerate matter. In OLN I we discussed the case where the ejected crust had insufficient angular momentum to escape the QS’s gravitational pull, and so would either balance with the QS’s magnetic field and form a co-rotating shell, or fall back entirely. Then in OLN II the case where the QS was born with a sufficient spin-period to impart the ejected crust with enough angular momentum to form a degenerate torus. In this paper, we explore the result of this degenerate torus after enough time has passed for it to expand to densities where it is non-degenerate.

2.1. Emission: Vortex Expulsion vs. Accretion

In our model the QS is in the ground Color-Flavor Locked (CFL) phase and so behaves as a type II superconductor, wherein a rotationally-induced lattice forms inside the star. As the star spins down the magnetic field, which is confined to exist only within the vortices, is also expelled and the subsequent magnetic reconnection leads to the production of X-rays. The luminosity from vortex expulsion is given in OLN I to be,

$$L_{X,v} \simeq 2.01 \times 10^{34} \text{ erg s}^{-1} \eta_{X,0.1} \dot{P}_{-11}^2. \quad (1)$$

Here the subscript v stands for “vortex” and $\eta_{X,0.1}$ is the efficiency parameter, in units of 0.1, inherent in the conversion from magnetic energy to observed radiation. The spin-down rate, \dot{P} is given in units of 10^{-11} s s $^{-1}$.

In this paper the degenerate material ejected during the quark-nova is imparted with sufficient angular momentum to form a degenerate torus, in which case accretion from this torus can result in emission that outshines the emission due to vortex

expulsion. The condition on the initial spin-period of the QS at birth is then an upper limit (from OLNII),

$$P_0 < P_{0,\max} = 2.5 \text{ ms} \frac{B_{0,15}^{3/2} R_{\text{QS},10}^{9/2}}{m_{0,-7}^{3/4} M_{\text{QS},1.4}^{5/4}}, \quad (2)$$

where $R_{\text{QS},10}$ is the radius of the QS in units of 10 km, $B_{0,15}$ is the initial magnetic field strength in units of 10^{15} G, and the initial mass of the torus is $m_{0,-7}$ in units of 10^{-7} solar masses. From here on, we parametrize the actual period as being some fraction, $\alpha_{0,3}$, of the maximum period in units of 0.3; $P_0 = \alpha P_{0,\max}$.

The accretion luminosity from the type of torus considered in this paper is given by equation (13) in OLNII,

$$L_{\text{X,acc.}} \simeq 1.7 \times 10^{33} \text{ erg s}^{-1} \frac{\eta_{0.1}^4 R_{\text{t},15}^6}{\mu_{3.3}^6 M_{\text{QS},1.4}^4}. \quad (3)$$

Here $\eta_{0.1}$ is the efficiency of conversion of accreted material into X-ray emission in units of 0.1, $R_{\text{t},15}$ is the radial distance of the torus in units of 15 km, $\mu_{3.3}$ is the mean molecular weight per electron in units of 3.3 (the quiescent phase value), and $M_{\text{QS},1.4}$ is the mass of the QS in units of 1.4 solar masses.

2.2. Degenerate Torus properties

The radius of the torus can be found from the initial spin-period of the QS as was done in OLNII,

$$R_{\text{t}} = 15 \text{ km} \alpha_{0.3}^{-8/3} P_{0,\text{ms}}^{2/3} M_{\text{QS},1.4}^{1/3}, \quad (4)$$

where the initial period is in units of milliseconds.

By assuming a constant accretion rate, the evolution of the torus mass can be determined, and the time needed for the torus to reach a density where it becomes non-degenerate is,

$$\tau_{\text{t}} \simeq \frac{m_0}{\dot{m}_{\text{t}}} \sim 3.4 \times 10^5 \text{ yrs} \frac{m_{0,-7} M_{\text{QS},1.4}^4 \mu_{3.3}^6}{\eta_{0.1}^3 R_{\text{t},15}^6}, \quad (5)$$

with \dot{m}_{t} being the torus accretion rate given by eq(10) in OLNII. The mass and density of the torus over time are plotted in Fig. 1.

While the torus is above degenerate densities, diffusion by the QS's magnetic field into the inner walls of the torus (leading to bursting accretion events; see OLNII) increases the inner radius. We can estimate the change inner radius of the torus, $R_{\text{in}} = R_{\text{t}} + \Delta R_{\text{t}}$ (see Appendix A), by using the typical time needed for magnetic field diffusion into the torus, τ_{B} , and the typical depth into the torus at which shear stresses become great enough such that accretion can proceed, Δr_{w} . Both of these parameters were estimated in OLNII (eqns. 17 & 5). We find that the change in inner radius over the span of the lifetime of the torus is negligible.

While the magnetic field slowly consumes the torus' inner edge, its outer edge moves outward (due to viscosity from particle collisions within a degenerate ideal gas) at a rate given by equation (A.7) in OLNII. After the time where the torus expands to densities at which it becomes non-degenerate, τ_{t} , the torus will have extended to an outer radius of,

$$R_{\text{out}} \simeq 207 \text{ km} \frac{m_{0,-7}^{1/2} M_{\text{QS},1.4}^2 \mu_{\text{q},3.3}^3}{\eta_{0.1}^{3/2} R_{\text{t},15}^{7/4}}, \quad (6)$$

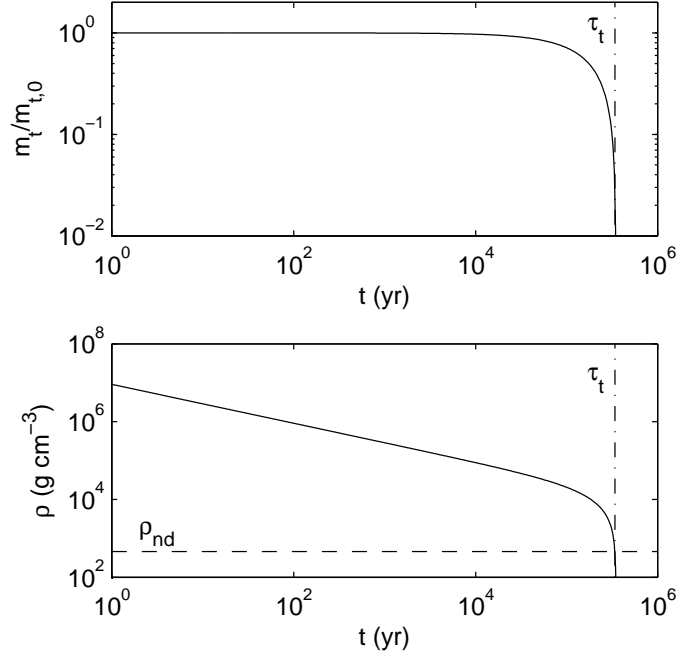


Fig. 1. The mass and density of the torus, assuming a temperature of 1 keV. τ_{t} and ρ_{nd} are the time and density at which the torus becomes non-degenerate.

3. Transition to RRAT phase

The evolution of the density of the torus (during its degenerate phase) is calculated using eq(A.8) in OLNII, and is shown in the lower panel in Fig. 1. At time τ_{t} , the torus density drops rapidly and eventually reaches densities that are below degeneracy. For temperatures estimated in the torus (eq. 13 in OLNII; $T_{\text{ev}} \simeq 85 \eta_{0.1} R_{\text{t},15} / M_{\text{QS},1.4}$), the density at which the torus makes the transition from degeneracy to non-degeneracy is, $\rho_{\text{nd}} \simeq 11.4 \text{ gm cm}^{-3} \eta_{0.1}^{3/2} R_{\text{t},15}^{3/2} / M_{\text{QS},1.4}^{3/2}$.

Upon the transition from degeneracy to non-degeneracy, the new viscosity becomes $\nu = 6.0 \times 10^{-4} T_{\text{ev}}^{5/2} \text{ cm}^2 \text{ s}^{-1}$ (OLNII eq. A.5). The corresponding accretion rate then is $\dot{m} \sim 0.0057 \text{ g s}^{-1} \rho_{\text{nd}} H_{\text{d}} T_{\text{ev}}^{5/2}$ which is completely negligible (Frank et al. (2002)); H_{d} is the disk thickness in units of centimeters. Thus, immediately following this transition the X-ray luminosity of the system is no longer dominated by accretion but rather by vortex (magnetic flux) expulsion from the star. The consequence of this would be a decrease in X-ray luminosity by a few orders of magnitude in a relatively short amount of time (see left panel in Figure 2).

3.1. Stellar properties

The evolution of the star's period and period derivative are defined by the physics of vortex expulsion (see Niebergall et al. (2006)),

$$P_{\text{QS}}(t) = P_{\text{QS},0} \left[1 + \frac{t}{\tau_{\text{v}}} \right]^{1/3}, \quad (7)$$

and

$$\dot{P}_{\text{QS}}(t) = \frac{P_{\text{QS},0}}{3\tau_v} \left[1 + \frac{t}{\tau_v} \right]^{-\frac{2}{3}}, \quad (8)$$

where

$$\tau_v = 840 \text{ s } B_{\text{QS},0,15}^{-2} P_{\text{QS},0,\text{ms}}^2 M_{\text{QS},1.4} R_{\text{QS},10}^{-4}, \quad (9)$$

is the characteristic age due to vortex expulsion. The other two important relations in our model are (see OLN I and OLN II)

$$B = \sqrt{3\kappa P \dot{P}} \\ PB^2 = P_0 B_0^2. \quad (10)$$

where $\kappa = 8.8 \times 10^{33} \text{ G}^2 \text{ s}^{-1}$. The former equation describes magnetic field decay while the latter allows us to link the initial and current conditions.

By making use of the above equations and equation (4), the star's period, period derivative, and magnetic field can be determined at the time, τ_t , when the transition to a non-degenerate torus is made (with $\tau_t \gg \tau_v$),

$$P_{\text{trans.}} \approx 2.3 \text{ s } \frac{\mu_{\text{q},3.3}^2 B_{0,15}^{4/3} M_{\text{QS},1.4}^{1/2} R_{\text{QS},10}^{10/3}}{\eta_{0.1} R_{\text{t},15}^{13/6}} \\ \dot{P}_{\text{trans.}} \approx 7.3 \times 10^{-14} \text{ s s}^{-1} P_{0,\text{ms}} \frac{\eta_{0.1}^2 R_{\text{t},15}^{13/3}}{\mu_{\text{q},3.3}^4 B_{0,15}^{2/3} M_{\text{QS},1.4}^2 R_{\text{QS},10}^{32/3}} \quad (11)$$

Combining equation above with eq.(10) we find $B_{0,15} \approx 2.1 f_* P_{\text{trans.},3}^{35/38} \dot{P}_{\text{trans.},-13}^{13/38}$ with $P_{\text{trans.}}$ and $\dot{P}_{\text{trans.}}$ in units of 3 s and $10^{-13} \text{ s s}^{-1}$, respectively, while $f_* = (R_{\text{QS},10}^{10} \mu_{\text{q},3.3} M_{\text{QS},1.4}^{-1/3} \eta_{0.1}^{-6/13} \alpha_{0.3}^{8/3})^{-39/76}$ is of order unity. Equations (4) and (11) give us $R_{\text{t},15}$ and $P_{0,\text{ms}}$. With $P_{0,\text{ms}}$, $B_{0,15}$ and eq(2) together, we solve for $m_{0,-7}$.

Table 2 shows birth parameters of the 3 RRATs studied here for $\alpha = 0.3$. We find an initial magnetic field $10^{14} < B_0 \text{ G} < 10^{16}$ and sub-millisecond birth periods. Also listed in Table 2 are the torus' initial inner radius, R_t , and initial mass, m_0 which implies $10^{-8} M_\odot < m_0 < 10^{-5} M_\odot$ and $10 < R_t \text{ (km)} < 35$.

3.2. Non-degenerate disk properties

The non-degenerate disk's thickness at a radial distance r is given by $H_d = v_{\text{th}}^2/g$, where $g = GM_{\text{QS}}H_d/r^3$ is the effective gravity at r , and $v_{\text{th}} = \sqrt{kT/(\mu_{\text{q}} m_{\text{H}})} \sim 1.7 \times 10^7 \text{ cm s}^{-1} \mu_{\text{q},3.3}^{-1/2} T_{\text{keV}}^{1/2}$, is the disk thermal speed. Thus, at R_{in} , we find

$$H_d \sim 3.9 \times 10^4 \text{ cm } \frac{T_{\text{d,keV}}^{1/2} R_{\text{in},100}^{3/2}}{\mu_{\text{q},3.3}^{1/2} M_{\text{QS},1.4}^{1/2}}, \quad (12)$$

while the disk's thickness is a few hundred meters at its outer edge, R_{out} . However, as we show below, the disk quickly cools reducing its temperature and thus its thickness until it solidifies. The density would continue dropping below ρ_{nd} until it reaches the density of normal iron $\rho_{\text{Fe}} \sim 7.86 \text{ g cm}^{-3}$.

The thermal evolution of the disk is given by,

$$C_v \frac{\partial T}{\partial t} = \frac{\Omega_d}{4\pi} L_{\text{X,v}} - L_{\text{BB,t}}, \quad (13)$$

where $\Omega_d = (2\pi H_d/R_d)$ is the solid angle extended by the disk with thickness H_d . In the above, C_v is the torus heat capacity while $L_{\text{BB,t}} \approx 2\pi R_{\text{out}}^2 \sigma T^4$ is the torus blackbody cooling. The disk cools, while H_d decreases, yielding smaller Ω_d thus further cooling. However, the decrease in H_d stops when the disk gas condenses which occurs at a temperature of $T_{\text{Fe,cond.}} \approx 0.265 \text{ eV}$ (CRC tables), since the disk composition is dominated by iron (see OLN I and OLN II).

To find the disk's thickness at the condensation point we impose conservation of surface density so that $H_d \rho_{\text{nd}} = H_{\text{d,cond.}} \rho_{\text{Fe}}$; we assume the surface density constant during the gas phase since the gas phase is short-lived so that

$$H_{\text{d,cond.}} \sim 0.12 \text{ cm } \frac{R_{\text{in},100}^{3/2}}{\mu_{\text{q},3.3}^{1/2} M_{\text{QS},1.4}^{1/2}}. \quad (14)$$

The solid disk is extremely thin varying from a millimeter (paper thin) at R_{in} up to a few centimeters at its outer edge.

Using $\Omega_{\text{d,cond.}} = (2\pi H_{\text{d,cond.}}/R_{\text{in}})$, we estimate the equilibrium temperature of the condensed disk to be

$$T_d \sim 18.6 \text{ meV } \frac{R_{\text{in},100}^{1/8} \dot{P}_{-13}^{1/2} \eta_{\text{X},0.1}^{1/4}}{R_{\text{out},1000}^{1/2} \mu_{\text{q},3.3}^{1/8} M_{\text{QS},1.4}^{1/8}}, \quad (15)$$

where R_{out} is given in units of 1000 km. For the 3 RRATs in the order listed in Tables we get, $\sim 6 \text{ meV}$, $\sim 86 \text{ meV}$ and $\sim 5.7 \text{ meV}$, respectively. At temperatures below 0.1 eV, condensed iron is in the form of ferrite, or α -iron, a body-centered cubic structure.

4. RRAT-like sporadic behavior

The inner disk will be slowly penetrated by the QS's magnetic field on timescales determined by the induction equation,

$$\frac{\partial B}{\partial t} = \frac{c^2}{4\pi\sigma} \nabla^2 B. \quad (16)$$

Here, $\sigma = n_{\text{e,th}} e^2 \lambda_e / (m_e v_{\text{rms}})$ and $\lambda_e = 1/(n_{\text{e,th}} \sigma_T)$, where $n_{\text{e,th}}$ is the number density of thermal electrons in the disk, σ_T is the Thompson scattering cross-section, and the root-mean-square electron velocity is $v_{\text{rms}} = v_{\text{th}}$. Therefore, the time needed for the magnetic field to penetrate to a depth of the order of $H_{\text{d,cond.}}$,

$$\tau_B \sim 1.3 \text{ hrs } \frac{R_{\text{in},100}^3}{T_{\text{d,meV}}^{1/2} \mu_{\text{q},3.3}^{1/2}}. \quad (17)$$

Once penetrated the inner disk is accreted, on free-fall timescales, onto the star along the magnetic field lines with

$$t_{\text{acc}} = \frac{R_{\text{in}}}{v_{\text{ff}}} \sim 2.3 \text{ ms } \frac{R_{\text{in},100}^{3/2}}{M_{\text{QS},1.4}^{1/2}}, \quad (18)$$

where $v_{\text{ff}} = \sqrt{2GM_{\text{QS}}/R_{\text{in}}}$ is the free-fall velocity.

Table 1. Observational properties of the RRATs.

Source	Star			Radio		
	P (s) ¹	\dot{P} (10^{-13} s s ⁻¹) ¹	L_X (erg s ⁻¹) ²	t_{on} (ms) ¹	t_{off} (hr) ¹	L_{radio} (erg s ⁻¹) ³
RRAT J1317–5759	2.6	0.126	$< 7.5 \times 10^{32}$	10	0.22	1.4×10^{31}
RRAT J1819–1458	4.3	5.76	3.3×10^{33}	3	0.057	5.6×10^{31}
RRAT J1913+3333	0.92	0.0787	$< 9.4 \times 10^{34}$	2	0.21	2.5×10^{31}

¹From McLaughlin et al. (2006); ²The observed X-ray luminosity (Reynolds et al. 2006); ³The observed radio luminosity assuming a bandwidth of 1 GHz (Rea (2007))**Table 2.** Birth parameters predicted by our model (for $\alpha = 0.3$).

Source	Star			Torus	
	B_0 (10^{15} G)	P_0 (ms)	\dot{P}_0 (10^{-6} s s ⁻¹)	R_t (km)	m_0 ($10^{-7} M_\odot$)
RRAT J1317–5759	0.91	0.27	1.2	13.4	3.3
RRAT J1819–1458	5.4	0.97	12	31.5	20
RRAT J1913+3333	0.30	0.20	0.18	10.8	0.53

Table 3. RRATs era parameters predicted by our model (for $\alpha = 0.3$).

Source	Star		Disk			Radio		
	$L_{X,v}$ (erg s ⁻¹)	T_{BB} (eV)	R_{in} (km)	R_{out} (km)	T_d (meV)	$t_{\text{on}} = t_{\text{acc.}}$ (ms)	$t_{\text{off}} = \tau_B$ (hr)	L_{Radio} (erg s ⁻¹)
RRAT J1317–5759	3.19×10^{28}	14	96	1082	6.0	2.2	0.46	3.3×10^{31}
RRAT J1819–1458	6.7×10^{31}	100	33	203	86	0.44	0.005	2.3×10^{30}
RRAT J1913+3333	1.25×10^{28}	11	132	820	5.7	3.5	1.2	7.1×10^{31}

 L_X from eq(1), T_{BB} from eq(20), R_{in} from eq(A.2), R_{out} from eq(6), T_d from eq(15), t_{acc} from eq(18), τ_B from eq(17), L_{radio} from eq(19) with $A_{\text{casc.}} = 10^2$.**Table 4.** (Torus and RRATs) Era duration predicted by our model (for $\alpha = 0.3$).

Source	τ_{torus} (yrs)	τ_{rrat} (yrs)
RRAT J1317–5759	2.2×10^6	7.9×10^5
RRAT J1819–1458	7.9×10^4	3.2×10^3
RRAT J1913+3333	1.3×10^6	4.1×10^5

 τ_{torus} from eq.(5); τ_{rrat} from eq.(24).

4.1. Radio emission mechanism and fluxes

Radio emission in our model is triggered by the accretion of the inner ring of mass $\Delta m_d \sim 2\pi R_{\text{in}} H_{\text{d,cond}}^2 \rho_{\text{Fe}}$. Each iron nucleon accreted leads to the generation of a GeV photon thus triggering a photon-pair cascade amplifying the accretion energy by a factor $A_{\text{casc.}}$.

The luminosity in radio is then $L_{\text{radio}} = A_{\text{casc.}}(0.1 \Delta m c^2)/t_{\text{acc.}}$, or,

$$L_{\text{radio}} \sim A_{\text{casc.}} 3.7 \times 10^{29} \text{ erg s}^{-1} \frac{R_{\text{in},100}^{5/2}}{\mu_{\text{q},3.3} M_{\text{QS},1.4}^{1/2}}. \quad (19)$$

As shown in Table 3, the observed radio fluxes can be accounted for consistently for all 3 candidates if an amplification factor of the order of 10^2 is assumed (a multiplicity number for secondary pairs can be as high as 10^5 ; e.g. Melrose 1995 and references therein). We expect the medium to be transparent to radio since it would most likely be emitted much above the polar region. We assume all radio bursts originate at the same longitude on the quark star. This guarantees that the bursts are modulated at the spin period, consistent with the assumption required to derive P and \dot{P} from the observations of RRATs.

Table 3 lists parameters derived from our model as compared to observations which shows some encouraging agreement with measured radio burst timescale and quiet phases. The case of RRAT J1819–1458 shows smaller bursting time and quiet time, as well as smaller radio fluxes probably because our model somehow predicts a smaller R_{in} than the actual one. For example, using $R_{\text{in}} \sim 80$ km instead of 33 km (i.e. $\alpha \sim 0.2$ instead of $\alpha = 0.3$) we find much better agreement.

5. Model Predictions

5.1. The two blackbodies

One of the key aspects of the transition from degenerate torus to a non-degenerate disk is the shutting-off of accretion thus eliminating one of the two BBs inherent to the accretion era (see OLNII). RRATs should show one dominant blackbody emission at a temperature given by

$$T_{\text{BB}} = (L_{X,v}/(4\pi R_{\text{QS}}^2 \sigma))^{1/4} \sim 0.04 \text{ keV} \dot{P}_{-13}^{1/2}, \quad (20)$$

where \dot{P} is in units of 10^{-13} s s⁻¹, and a dimmer one at T_d representing the remnant iron disk. In particular, for RRAT J1819–1458 for which $\dot{P}_{-13} = 5.76$ we predict $T_{\text{BB}} \sim 0.1$ keV and

another blackbody in infrared at ~ 940 K. The blackbody temperature for the other two candidates are listed in Table 3 which shows a BB temperature in the ultra-violet region and disk temperatures in the Infrared, 50-100 K.

5.2. Absorption lines

Since the disk is cooler than the star ($T_d < T_{BB}$), it will act as an absorber of the blackbody emission. The column density in the inner part of the disk is

$$N_{d,Fe} = \frac{H_{d,cond} \rho_{Fe}}{56 m_H} \sim 10^{22} \text{ gm cm}^{-2} R_{in,100}^{3/2}, \quad (21)$$

high enough to lead to absorption. The X-ray spectrum of RRAT J1819–1458 showed a single blackbody component did not fit the data because of the presence of two strong absorption features around 0.5 and 1 keV (Rea (2007)). In our model, these may be explained as absorption lines due the disk.

5.3. Increase in spin-down rate when radio is on

During the quiet period the star's spin-down rate is simply given by $\dot{P} = P/(3t_{age})$ where t_{age} is the source age. However, it is natural to expect spin-down increase during the on era since the polar wind (secondary pairs) act as a torque against the star's rotation.

The angular momentum per unit mass lost at the light cylinder is c^2/Ω_{QS} , which enhances the spin-down rate of the quark star during radio bursts to, using $(\Delta m_d/t_{acc})c^2/\Omega_{QS} \approx I_{QS}\dot{\Omega}_{QS}$, I_{QS} is the star's moment of inertia,

$$\Delta \dot{P} \approx 6.7 \times 10^{-17} \text{ s s}^{-1} \frac{P^3 R_{in,100}^{5/2}}{M_{QS,1.4} R_{QS,10}^2}. \quad (22)$$

Compared to $\dot{P}_{trans.}$ we get

$$\frac{\Delta \dot{P}}{\dot{P}_{trans.}} \sim 9.2 \times 10^{-4} \frac{P^3 R_{in,100}^{5/2} B_{0,15}^{2/3}}{P_{0,ms} R_{t,15}^{13/3}} \quad (23)$$

As can be seen from the equation above the increase in spin-down rate when radio is on is negligible is negligible. However, as we show below, as the RRAT ages the increase in spin-down rate during the on period is noticeable.

5.4. Old RRATs: the case of PSR B1931+24

A simple estimate of the lifetime of a RRAT can be found by integrating equation $dt/dr \approx \tau_B/H_{d,cond.}$, from R_{in} to R_{out} , to get

$$\tau_{rrat} \sim 1.6 \times 10^6 \text{ yrs} \frac{R_{out,1000}^{5/2}}{T_{d,mcV}^{1/2}}. \quad (24)$$

The late stages of the RRAT ($\tau_{rrat} \sim 10^6$ yrs) era, correspond to the era when the magnetic field is consuming the last outermost remnants of the disk; i.e. when the disk radius is close to R_{out} .

When the radio is off (no accretion) the star spins-down via vortex expulsion with a period derivative given by $\dot{P} =$

$P/(3\tau_{rrat})$. Using equations (24) and (15) with $R_{in} \sim R_{out}$, we get

$$\dot{P}_{off} \sim 2.3 \times 10^{-14} \text{ s s}^{-1} P^{4/3} R_{out,1000}^{-43/12}, \quad (25)$$

The increase in spin-down rate during the on period, is found by replacing $R_{in} \sim R_{out}$ in eq.(22), so that

$$\Delta \dot{P} \approx 2.1 \times 10^{-14} \text{ s s}^{-1} \frac{P^3 R_{out,1000}^{5/2}}{M_{QS,1.4} R_{QS,10}^2}. \quad (26)$$

The spin-down rate during the on era is thus $\dot{P}_{on} = \dot{P}_{off} + \Delta \dot{P}$.

The observed periodicity of the radio-on and radio-off recurrence of PSR B1931+24 (Kramer et al. (2006)Kramer, Lyne, O'Brien, Jordan, and Lorimer) is difficult to explain in any scenario considering an isolated pulsar, and as Kramer et al. (2006)Kramer, Lyne, O'Brien, Jordan, and Lorimer pointed out, the short shut-off time of less than 10 seconds, rules out possible scenarios like precession of the neutron star. Furthermore, the facts that the off periods of PSR B1931+24 are five orders of magnitude longer than typical nulling periods, that the activity pattern is quasi-periodic and that not a single null has been observed during on periods strongly argues against the nulling scenario. It appears however that magnetospheric conditions are sufficient to explain the change in the neutron star torque, but it is not clear what determines the ~ 30 -40 days periodicity or what could be responsible for changing the plasma flow in the magnetosphere, in particular in this quasi-periodic fashion.

Assuming PSR B1931+24 ($P = 0.813$ s) is an old RRAT that is currently consuming the outermost part of its disk, our model implies a corresponding spin-down frequency during the off period of $\dot{\nu}_{off} = -\nu^2 \dot{P}_{off} \approx -2.6 \times 10^{-14} \text{ Hz s}^{-1}$, while during the on period the increase in spin-down frequency is $\Delta \dot{\nu} \approx -1.7 \times 10^{-14} \text{ Hz s}^{-1}$. It means an increase of about 65% in spin-down rate during the on period so that $\dot{\nu}_{on} \approx -4.3 \times 10^{-14} \text{ Hz s}^{-1}$. Our numbers are remarkably similar to what has been measured for PSR B1931+24. For this source the observed spin-down rate the pulsar rotation slows down 50% faster when it is on than when it is off with $\dot{\nu}_{off} = -1.08 \times 10^{-14} \text{ Hz s}^{-1}$ while $\dot{\nu}_{on} = -1.63 \times 10^{-14} \text{ Hz s}^{-1}$.

For PSR B1931+24 the quiet period last for ~ 30 -40 days while the active period is of the order of ~ 5 days. In our model, the timescales for the bursting and quiet phases in old RRATs are $t_{acc.} \sim 70$ ms and $\tau_B \sim 50$ days. While the off period is again remarkably similar to the observed one, the observed on period of ~ 5 days is difficult to reconcile with our model which predicts ~ 70 ms. It is worth noticing however that Kramer et al. (2006)Kramer, Lyne, O'Brien, Jordan, and Lorimer have been able to observe one switch from on to off that occurred within less than 10 seconds (although switches between the on and off states are rare events). This number is rather closer to $t_{acc.}$ in our model than to the radio-on timescale. It might be possible that another mechanism is at play delaying the accretion onto the pole. Finally, the corresponding radio flux in our model is estimated to be $L_{radio} \sim 10^{34} \text{ erg s}^{-1}$.

5.5. XDINs and “dead” RRATs in our model

Some XDINs might be direct descendants of Qs with shells (SGRs in our model; see Appendix B). These would have evolved along the “vortex” band since their birth. However, as illustrated in Figure 2, some XDINs might be dead RRATs. That is, they fell into the “vortex” band following torus consumption and eventually evolved along the band. The main difference between SGR-descendants XDINs and AXP-descendant XDINs (dead RRATs) is the possibility of remnant disk surrounding the AXP-descendant XDINs. We thus expect some of the XDINs to share some common properties with RRATs such as optical (or Infrared) excess. Broad absorption lines, similar to those seen for RRAT J1819–1458, have been observed for six out of seven XDINs (van Kerkwijk & Kaplan 2007; Haberl 2007). We have already argued in OLNII that these absorption lines are caused by absorption from an old, cold disk (see also §5.2).

At first glance the birth rates of RRATs as descendants of AXPs in our model, appears to be too low to explain the high inferred population (McLaughlin et al. 2006) of a few times (~ 5) that of radio pulsars. Taking the RRAT birth rate to be that of AXPs, i.e. $\sim 1/(500 \text{ yrs})$ (Leahy & Ouyed 2007 and references therein), implies a birth rate of $\sim 1/10$ of that of radio pulsars. In order to have a RRAT population ~ 5 times the radio pulsar population, the RRAT lifetime must be ~ 50 times longer than that of a radio pulsar ($\sim 10^6 \text{ yrs}$). In our model, the RRAT lifetime estimate, given by eq.(24), is of order a few million years. However, this is strongly dependent on R_{out} . An R_{out} larger by a factor of 4 (caused by different effects; see eq.(6)) gives a large enough RRAT lifetime, i.e. a low enough birth rate.

6. Conclusion

Here we have presented a model where RRATs fit in naturally as descendants of AXPs with degenerate iron-rich disks, with the transition occurring when the disk becomes non-degenerate. These AXPs in our model are the quark star remnants of quark-novae, surrounded by the ejected former neutron star’s crust material. The evolution of quark stars as they spin down is summarized in the L_X - \dot{P} diagram in Figure 2 (see appendix B). Although this model is speculative, it can explain many features of SGRs and AXPs (OLNI and OLNII) and RRATs.

Acknowledgements. Youling Yue thanks the University of Calgary for hosting him during this work. This research is supported by grants from the Natural Science and Engineering Research Council of Canada (NSERC). Youling Yue is supported by the State Scholarship Fund of China

References

Chatterjee, P., Hernquist, L., & Narayan, R. 2000, *Astrophysical Journal*, 534, 373
 Cordes J. M. & Shannon, R. M. 2006, *ApJ*, submitted (astro-ph/0605145)
 Cordes J. M., Lazio, T. J. W., & McLaughlin M. A. 2004 *New Astronomy Reviews*, 48, 1459

Dyks J., Zhang B., & Gil, J. 2005, *ApJ*, 626, L45
 Ertan, Ü., Göğüş, E., & Alpar, M. A. 2006, *Astrophysical Journal*, 640, 435
 Frank, J., King, A., & Raine, D. J. 2002, *Accretion Power in Astrophysics*, Cambridge, UK: Cambridge University Press, 3rd ed.
 Gaensler, B. M., et al. 2007, *Astrophysics and Space Science*, 308, 95
 Gil J. A., Jessner A., Kijak J. et al. 1994 *A&A*, 282, 45
 Gonzalez M. E., Kaspi V. M., Camilo F., et al. 2005, *ApJ*, 630, 489
 Gotthelf E. V., Halpern J. P., Buxton M., & Bailyn C. 2004, *ApJ*, 605, 368
 Hyman S. D., Lazio T. J. W., Kassim N. E., et al. 2005, *Nature*, 434, 50
 Ibrahim A. I., Markwardt C. B., Swank J. H., et al. 2004, *ApJ*, 609, L21
 Jackson, J. D. 1975, *Classical electrodynamics*, New York: Wiley, 2nd ed.
 Kaplan D. L., Frail D. A., Gaensler B. M., et al. 2004, *ApJS*, 153, 269
 Kaspi V. M., & McLaughlin M. A. 2005, *ApJ*, 618, L41
 Keränen, P., & Ouyed, R. 2003, *Astronomy & Astrophysics*, 407, L51
 Keränen, P., Ouyed, R., & Jaikumar, P. 2005, *Astrophysical Journal*, 618, 485
 Kramer M., Lyne A. G., O’Brien J. T., et al. 2006, *Science*, 312, 549
 Kondratiev, V. I. et al. 2007, *arXiv:0710.1648*
 Leahy, D., & Ouyed, R. 2007a, *ArXiv e-prints*, 708, *arXiv:0708.1787*
 Leahy, D., & Ouyed, R. 2007b, *ArXiv e-prints*, 710, *arXiv:0710.2114*
 Lewandowski W., Wolszczan A., Feiler G., et al. 2004, *ApJ*, 600, 905
 Li, X.-D. 2006, *ApJ*, 646, L139
 Lugones, G., Benvenuto, O. G., & Vucetich, H. 1994, *Phys. Rev. D*, 50, 6100
 Luo, Q., & Melrose, D. 2007, *Monthly Notices of the Royal Astronomical Society*, 378, 1481
 McLaughlin M. A., Lyne A. G., & Lorimer D. R., et al. 2006, *Nature*, 439, 817
 Melrose, D. B. 1995, *J. Astrophys. Astr.* 16, 137
 Niebergal, B., Ouyed, R., & Leahy, D. 2006, *Astrophysical Journal Letters*, 646, L17
 Niebergal, B., Ouyed, R., & Leahy, D. 2007, *ArXiv e-prints*, 709, *arXiv:0709.1492*
 Ouyed, R., Dey, J., & Dey, M. 2002, *A&A*, 390, L39
 Ouyed, R., Elgarøy, Ø., Dahle, H., & Keränen, P. 2004, *Astronomy & Astrophysics*, 420, 1025
 Ouyed, R., Niebergal, B., Dobler, W., & Leahy, D. 2006, *Astrophysical Journal*, 653, 558
 Ouyed, R., Leahy, D., & Niebergal, B. 2007a, *Astronomy & Astrophysics*, 473, 357 (OLNI)
 Ouyed, R., Leahy, D., & Niebergal, B. 2007b, *Astronomy & Astrophysics*, 475, 63 (OLNII)
 Ouyed, R., et al. 2007, *Submitted to ApJ* [astro-ph/0705.1240]
 Popov, S. B., Turolla, R., & Possenti, A. 2006, *Monthly Notices of the Royal Astronomical Society*, 369, L23
 Rea, N. 2007, *arXiv:0710.2056*
 Reynolds, S. P., et al. 2006, *Astrophysical Journal Letters*, 639, L71
 Wang, Z., Chakrabarty, D., & Kaplan, D. L. 2006, *Nature*, 440, 772
 Weltevrede P., Stappers B. W., Rankin J. M., & Wright G. A. E. 2006, *ApJ*, 645, L149
 Zhang, B., Gil, J., & Dyks, J. 2007, *Monthly Notices of the Royal Astronomical Society*, 374, 1103

Appendix A: Evolution of torus inner radius

During the degenerate phase, the inner walls of the torus are carved out by magnetic penetration (leading to bursting accretion events; see OLNII) increasing the inner radius from R_i to

B.3. Statistical appearance of SGRs

In our model, features and statistics of SGRs can be accounted for if they are born (via the quark-nova mechanism) from 200 ms neutron star progenitors. The statistical line² for 200 ms (shell harboring) sources in our model is, with a birth rate of one per 500 yrs (as estimated by Leahy & Ouyed (2007b)),

$$\begin{aligned} P_{\text{stat.,200}} &\sim 1.2 \text{ s } B_{0,15}^{2/3} P_{0,200 \text{ ms}}^{1/3} R_{\text{QS},10}^{4/3} M_{\text{QS},1.4}^{-1/3} \\ \dot{P}_{\text{stat.,200}} &\sim 6 \times 10^{-11} \text{ s s}^{-1} B_{0,15}^{2/3} P_{0,200 \text{ ms}}^{1/3} R_{\text{QS},10}^{4/3} M_{\text{QS},1.4}^{-1/3}. \end{aligned} \quad (\text{B.2})$$

If we adopt an initial magnetic field strength of $B_0 = 10^{16}$ G for the 200 ms objects we find a statistical line at $P_{\text{stat.,200}} \sim 5.3$ s and $\dot{P}_{\text{stat.,200}} \sim 2.7 \times 10^{-10} \text{ s s}^{-1}$, which is to the right of SGRs location in the L_X - \dot{P} diagram. In fact for these objects, as they evolve to lower \dot{P} the shell is consumed and they become less active. Thus our earlier suggestion (OLNI and OLNII) that what is referred to as AXPs in the literature are old shell-harboring sources in our model that consumed most of their shell.

B.4. Statistical appearance of AXPs

The statistical line for millisecond (torus harboring) sources is given by eqs. (7) and (8) in our model (for $t \sim 500$ yrs):

$$\begin{aligned} P_{\text{stat.,1}} &\sim 0.2 \text{ s } B_{0,15}^{2/3} P_{0,\text{ms}}^{1/3} R_{\text{QS},10}^{4/3} M_{\text{QS},1.4}^{-1/3} \\ \dot{P}_{\text{stat.,1}} &\sim 10^{-11} \text{ s s}^{-1} B_{0,15}^{2/3} P_{0,\text{ms}}^{1/3} R_{\text{QS},10}^{4/3} M_{\text{QS},1.4}^{-1/3} \end{aligned} \quad (\text{B.3})$$

However as can be seen in the right panel of Figure 2, all AXPs are to the right of the above derived statistical line. As we will argue below, all of the observed sources to the right of the $10^{-11} \text{ s s}^{-1}$ line are SGRs (shell harboring quark stars in our model) with different shell masses with older ones having smaller shells thus with fewer and less energetic bursts (see OLNI).

Torus-harboring sources in our model are first seen at periods of ~ 0.2 s and period derivative of the order of $10^{-11} \text{ s s}^{-1}$. We thus predict a population of AXPs with sub-second period and an X-ray luminosity $\sim 10^{34} \text{ erg s}^{-1}$, from eq(1).

B.5. SN transparency line

For completeness, we also define a transparency line related to the time needed for a supernova remnant to be transparent to X-ray. A rough estimate gives

$$t_{\text{SN,transp.}} \sim 2 \text{ yr } M_{\text{SN},10} v_{\text{SN},4000}^{-2}, \quad (\text{B.4})$$

for a SN ejecta of mass $10M_\odot$ and velocity of 4000 km s^{-1} . In our model, for AXPs ($P_{0,\text{ms}} \sim 1$ and $B_{0,15} \sim 1$) we get $P_{\text{SN,transp.}} \sim 39 \text{ ms}$ and $\dot{P}_{\text{SN,transp.}} \sim 2.3 \times 10^{-10} \text{ s s}^{-1}$. For SGRs ($P_{0,\text{ms}} \sim 200$ and $B_{0,15} \sim 10$), we find $P_{\text{SN,transp.}} \sim 1.1 \text{ s}$ and $\dot{P}_{\text{SN,transp.}} \sim 6 \times 10^{-9} \text{ s s}^{-1}$.

² The statistical line is the age of the youngest observed source in a population: $\text{age} \sim 1/B$ for birthrate B .